NASA
Technical
Paper
2481

October 1985

A Study of the Cornering Forces Generated by Aircraft Tires on a Tilted, Free-Swiveling Nose Gear

Robert H. Daugherty
and Sandy M. Stubbs

NASA

NASA Technical Paper 2481

1985

A Study of the Cornering Forces Generated by Aircraft Tires on a Tilted, Free-Swiveling Nose Gear

Robert H. Daugherty
and Sandy M. Stubbs

Langley Research Center
Hampton, Virginia

National Aeronautics
and Space Administration

Scientific and Technical Information Branch

Summary

An experimental investigation was conducted at the NASA Langley Research Center to study the effects of various parameters on the cornering forces produced by a rolling aircraft tire installed on a tilted, free-swiveling nose gear. The parameters studied included tilt angle, trail, tire inflation pressure, rake angle, vertical load, and in the case of twin tires, whether or not they corotate. These parameters were evaluated by measuring the cornering force produced by an aircraft tire installed on the nose gear of a modified vehicle as it was towed slowly.

Although more readily apparent in a corotating twin-tire system, this cornering-force phenomenon occurs in a single tire when a tilt angle causes one side of the tire to have a smaller rolling radius than the other side and thus creates a differential slip in the tire footprint.

In general, the cornering-force coefficient increases as tilt angle increases. Increasing trail decreases the cornering-force coefficient nonlinearly for a given tilt angle. Tire inflation pressure has no effect on the cornering-force coefficient, whereas nose-gear rake decreases cornering-force coefficient. Increasing vertical load dramatically decreases the cornering-force coefficient at a fixed tilt angle. Having a twin-tire system does not affect the cornering-force coefficient if the tires can rotate independently. However, if the twin-tire system corotates, the cornering-force coefficient for a given tilt angle can be greatly increased.

Introduction

The mechanical characteristics of tires sometimes cause them to produce forces not normally anticipated. One such phenomenon involves a tire producing side or cornering forces when it rolls in a tilted condition and is free to pivot or swivel about the steering axis. This phenomenon was observed in 1966 during landing-gear tests conducted on a model of an HL-10 manned lifting entry vehicle (ref. 1). During these tests it was learned that asymmetrical main-gear strut deflection, which produced a tilt on all three landing-gear struts, led to development of side forces at the nose gear if it was free to swivel. It was demonstrated that this phenomenon could be used as an alternate steering method. Since publication of reference 1, however, this steering phenomenon has not been recognized by the aviation community in general.

Recently, excessive and unexplained differential braking forces were required on some Space Shuttle orbiter landings to keep the orbiter aligned with the runway centerline. It was determined that the combination of crosswinds and runway crown caused the orbiter to assume a roll or tilt angle, and since the nose gear is typically operated in a free-swiveling mode during rollout, unwanted cornering forces were developed at the nose gear.

The purpose of this paper is to present results of tests conducted at the NASA Langley Research Center to determine the cause of this cornering-force phenomenon. The paper also examines the effects of various parameters on the magnitude of cornering forces produced by a free-swiveling nose-gear tire rolling in a tilted attitude. These parameters include tilt angle, trail, tire inflation pressure, rake angle, vertical load, and in the case of a twin-tire arrangement, whether the wheels are locked together to rotate as a unit or are allowed to rotate independently.

Apparatus

Test Vehicle and Tires

The vehicle used in this investigation was a modified airboat shown in figure 1. A retractable tricycle landing gear was added to the airboat and provided a means for producing roll attitudes up to 10°. The airboat weighed 4425 lb, and the vertical load on the nose gear was typically 480 lb, except for tests examining the effect of vertical load, during which weights were added to the nose gear. A more detailed description of the vehicle can be found in reference 2. The lateral distance between the main gears was approximately 11 ft, and the spacing between the nose gear and the main gear was 13.4 ft.

Several different nose-gear configurations were studied in this investigation. Inserts were added to the nose-gear piston to modify the standard zero-trail configuration to configurations of 1.5 and 10 in. of trail. Photographs of the zero-trail and 10-in.-trail configurations are shown in figure 2. In addition, tests were conducted on a twin-tire arrangement shown in figure 3. The distance between the wheel centerlines was 8 in. for the twin-tire arrangement. An insert for the nose-gear drag link was fabricated, and when installed, it produced a forward rake angle of 10° on the nose gear.

The nose-gear tires used in this investigation were 6.00 × 6 TT 8-ply type III aircraft tires with a rated load of 2350 lb. The main-gear tires were 6.50 × 10 TT 8-ply type III aircraft tires with a rated load of 3750 lb.

Towing System

A schematic of the towing system used in this investigation is shown in figure 4. The lead (tow) tug pulled both the test vehicle and the instrumentation tug; both tugs followed straight expansion joints on a flat concrete surface. A cable with an integral load cell was attached to the nose-gear cylinder and to the instrumentation tug. The test vehicle was tilted away from the instrumentation tug, so that the instrumented cable from the nose gear was always in tension. A portable generator provided

electrical power for the recording system mounted on the instrumentation tug.

Instrumentation

A strain-gauge-type load cell was used to measure the load in the cable between the test vehicle nose gear and the instrumentation tug. For four tests, a strain-gauge-type load cell was mounted in the left main-gear scissor assembly to obtain a measure of torque. The signals from these strain gauges were recorded in real time on a strip chart recorder.

Testing Technique

Before each towed run, the test vehicle and the two tugs were positioned, and all cables were secured. Next, the tilt angle for the test was set by raising or lowering each gear while maintaining the proper rake angle. The rake angle was normally set at 0°. Finally, an instrumentation calibration was performed, and the tow test began. All tow tests were conducted at a speed of approximately 5 ft/sec and covered a distance of approximately 200 ft on a level concrete apron.

Results and Discussion

The test conditions and results for each of the towed runs are summarized in table I. The first series of test results presented in the following paragraphs provides insights into the basic phenomenon of cornering-force generation by tilted tires and sheds light on the underlying mechanisms responsible for these forces. The effects of various parameters on the cornering force produced by an aircraft tire installed on a free-swiveling nose gear are also evaluated in the following paragraphs. These parameters include tilt angle, trail, tire inflation pressure, rake angle, tire vertical load as a function of rated load, and in the case of a twin-tire arrangement, whether or not the tires corotate. Definitions of some of the parameters and forces discussed in this paper are given in appendix A.

Generation of Cornering Forces by a Tilted Tire on a Free-Swiveling Nose Gear

Initial tests. The first set of data, represented by the circular symbols in figure 5, was obtained to evaluate the effect of tilt angle on tire cornering force. The tire was inflated to 24 psi and was loaded vertically to 480 lb, which represents 20 percent of the tire rated load. A linear curve-fitting technique was applied to the experimental data. A maximum cornering force of approximately 310 lb was obtained for a tilt angle of 10°. Although the higher tilt angles, beyond 5°, would not be expected to occur on an aircraft under normal operations, they were included in this investigation to illustrate more vividly the cornering-force-generation phenomenon and to obtain a more accurate linear curve fit of the data at the lower tilt angles.

Nose-gear isolation tests. A series of tests was conducted to determine if the main gears of the test vehicle affected the force readings obtained at the nose gear. For these tests, a dolly was placed under the nose-gear tire, so that no cornering forces could be generated by the tire. Then tests were conducted at tilt angles up to 10°. The square symbols in figure 5 denote these forces as a function of tilt angle. Small cornering forces were observed for these test conditions, with a maximum force of about 25 lb at a tilt angle of 10°.

To verify the presence of these main-gear forces, another set of tests was conducted with a dolly under each main-gear tire, so that cornering forces could not be generated by those tires, and any force measurements obtained would be those generated strictly by the nose-gear tire. The results are also presented in figure 5 and are denoted by the triangular symbols. The resultant cornering forces are, in fact, lower than the original ones by the same 25 lb at a tilt angle of 10°. All following tests were conducted without dollies, and the measured nose-gear forces reported in this paper were adjusted to remove the effect of the main-gear forces at the rate of 2.5 lb/deg of tilt.

Differential slip within the tire footprint. The following free body diagram of the test vehicle during the test at a tilt angle of 10° with a dolly under the nose gear indicates that the main gears are producing a total force, $2F_m$, of 25 lb in the direction of the tilt:

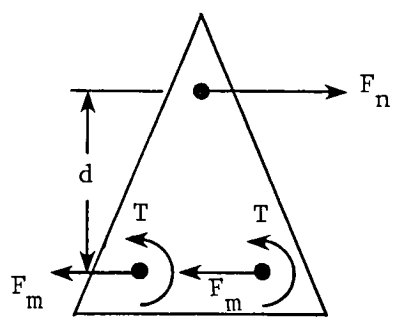

$$2F_m = F_n \qquad T = F_n d/2$$

The measured force, F_n, at the nose gear and the force produced by the main gears produced a couple on the test vehicle of 25 lb times the spacing between the nose gear and the main gear, d, of 13.4 ft, or 335 ft-lb. The test vehicle did not yaw during the test. The absence of yaw indicates that the main tires produced an opposing torque, $2T$. The assumption was made that each main

tire produced half of the opposing torque, which varied linearly from zero at no tilt to 167.5 ft-lb at a tilt angle of 10°.

A calibrated load cell was placed in one of the main-gear scissor assemblies to provide a measurement of the torque produced by one of the main-gear tires. Figure 6 presents plots of the measured main-gear torque and the predicted torque based on the free body diagram as a function of tilt angle. The prediction agrees very well with the experimental data. The data show that there is indeed a torque produced in the footprint of a tilted, rolling tire and that the mechanism that produces this torque is the basis for the generation of cornering forces due to tilt.

Another observation provided additional information on this phenomenon. This observation involved the appearance of the tire tracks of the main gear on the concrete test area after the vehicle was tested, especially at the larger tilt angles. The tires left rubber deposits, and in each track, the edge toward the direction of tilt was obviously darker. Thus, increased tire wear is indicated in this region of the tire contact area. This observation suggests that differential slip occurs across the footprint of a tilted, rolling tire.

To illustrate this differential slip more clearly, a piece of graph paper was lightly coated with grease, and a thin string was laid along one of the lines of the graph paper, as shown in figure 7. The vehicle was tilted to 10° and towed so that a main-gear tire rolled across the paper perpendicular to the string. The grease prevented the string from moving after the tire had rolled off the paper, and a visual indication was obtained of the differential slipping that developed in the tire footprint. Both the initial and final positions of the string are shown in figure 7. The final position of the string near the left edge of the footprint indicated that this portion of the footprint was in a slipping or braking condition. The final position of the string near the right edge of the footprint indicated that this side of the tire was in a spinning or driving condition. These results indicate that the mechanism by which tilted, rolling tires produce cornering force is differential slip. This differential slip is similar to that observed in corotating twin-tire systems. Corotation has classically been defined with respect to a twin-tire system, usually on a nose gear. Two tires are said to corotate if their wheels share a common axle and are forced to rotate at the same angular velocity. If such a system is tilted, one tire is more heavily loaded than the other, and a difference in rolling radius is produced. Since the tires corotate, the tire with the smaller rolling radius must slip, whereas the other tire must spin. The differential slipping creates a torque about the steering axis of the system, and if it is free to pivot, the system will tend to steer in the direction of the torque. The action of the tire rolling in a direction yawed to the direction of motion produces a side force which acts behind the steering axis, as shown in appendix B. The tires continue to steer in the direction of the torque until the moment produced by the side force acting behind the steering axis is balanced by the torque due to differential slipping. When this torque equilibrium is reached, an unbalanced force, the cornering force due to tilt, is present. This cornering force can be responsible for uncommanded steering inputs during aircraft ground operations. It should be noted that significant cornering forces due to tilt arise only when the nose gear is free to swivel. If the nose gear is locked or nose-gear steering is engaged, the torque produced by differential slipping is counteracted by the gear and aircraft structure, and cornering forces due to tilt are essentially eliminated.

As a result of this investigation, it was determined that substantial torques due to differential slipping can be developed by a single tire. The "common axle" is the wheel itself. Reference 3 suggests that a single tire can be treated as two thin tires separated by the tire width. For this analysis, the tire is treated as an infinite number of thin tires, each having a different rolling radius based on its lateral location in the tire footprint. A mathematical description of this approach can be found in appendix B.

Effects of Various Parameters on Cornering Forces Generated by Tilted Tires

Trail. The effect of trail on the cornering force generated by a tilted, rolling tire is illustrated in figure 8. Note that for the remainder of this paper, cornering force will be expressed as cornering-force coefficient, μ_c, determined by subtracting 2.5 lb/deg from each measured cornering force at the various tilt angles and dividing by the normal load on the nose gear for that test. The cornering-force coefficients were largest at zero trail and decreased with increasing trail over the range of tilt angles tested. This trend of decreasing cornering-force coefficient with increasing trail is attributed to a moment balance. If it is assumed that the torque due to differential slip produced by a tire at a fixed tilt angle is constant, then increasing trail would provide a longer arm through which smaller forces would be necessary to balance this torque.

To illustrate the nonlinear behavior of μ_c with respect to trail, figure 9 presents a plot of μ_c as a function of trail at various tilt angles. The data in the figure suggest the presence of an asymptotic relationship between μ_c and trail. One explanation for this asymptotic behavior may be that the side-force moment arm described in appendix B is a fraction of the total footprint length, and as trail increases, the ratio of this moment arm to the total trail becomes smaller and eventually insignificant, at which point a cornering-force limit has been reached. Note, however, that aircraft nose gears are not likely to be designed with so much trail that this asymptotic limit is reached.

Tire inflation pressure. Several tests were conducted to evaluate the effect of tire inflation pressure on the cornering forces generated by a tilted, rolling tire. Figure 10 presents a plot of cornering-force coefficient as a function of tilt angle for various tire inflation pressures and trails. Data obtained from previous tests at zero trail and at an inflation pressure of 24 psi, denoted by the circular symbols, are replotted, along with data at an inflation pressure of 60 psi, denoted by the square symbols. These tests were conducted at a vertical load of 480 lb, and the tire was operating in its normal deflection range. Inflation pressure had no effect on the cornering-force coefficient. This behavior may again be attributed to a moment balance. As tire inflation pressure increases, tire footprint width decreases, and a lower torque due to differential slipping is produced. However, the side-force moment arm also decreases as a result of decreasing tire footprint length, and the same side force is required to act at a new fore and aft position to balance the torque.

Another set of tests was conducted at 1.5 in. of trail at a tire inflation pressure of 12 psi. These data, denoted by the diamond symbols in figure 10, are compared with data previously obtained at 24 psi, denoted by the triangular symbols. The cornering-force coefficient at an inflation pressure of 12 psi is less than that at 24 psi. The reason for this behavior is most likely underinflation of the tire at 12 psi. Thus, the load produced excessive tire deflection past the design limit of approximately 35 percent. In this case the tire did not behave as expected and produced less cornering force than normal.

Rake angle. One set of tests was conducted with the nose-gear strut raked forward at an angle of 10° to evaluate the effect of rake on the cornering-force coefficient developed by a tilted tire. The results of the forward rake tests, denoted by the square symbols, are plotted in figure 11, along with data obtained at zero rake, denoted by the circular symbols. Both sets of data were obtained with 1.5 in. of trail. Rake angle reduces the cornering-force coefficient at a given tilt angle, with a reduction of about 14 percent at a forward rake angle of 10°.

Vertical load. Steering forces developed by a yawed, rolling tire are sensitive to variations in the vertical load (refs. 4 and 5). A series of tests was conducted to determine if this effect was also associated with the cornering forces developed by a tilted, rolling tire. Tests were conducted on a single tire at vertical loads of 480, 980, and 1760 lb, representing 20, 42, and 75 percent of the tire rated load, respectively. All tests were conducted with a trail of 1.5 in. The results of these tests are plotted in figure 12. As the vertical load on the tire is increased, the slope of the cornering-force-coefficient curve decreases from 0.041/deg at 20 percent of the rated load to 0.022/deg at 75 percent of the rated load. This indicates that as the tire deflection increases due to increased load, the tire becomes less efficient at producing cornering force at a given tilt angle. This behavior is very similar to that observed in references 4 and 5 and suggests that the response of a tilted tire may be similar to the response of a yawed tire for other parameters as well.

Independently rotating twin tires. Several tests were conducted to determine the effect of a twin-tire nose-gear arrangement on the magnitude of the cornering forces developed at the nose gear. The first test series was conducted with the twin-tire arrangement designed to allow each tire to rotate independently. (See fig. 3.) The vertical load on the nose gear for these tests was 480 lb and represents 10 percent of the rated load for each of the twin tires compared with 20 percent of the rated load for a single tire. Figure 13 presents a plot of cornering-force coefficient as a function of the tilt angle for both 1.5 and 10 in. of trail. Twin-tire data are compared with previously presented single-tire data. The data indicate that the cornering-force coefficients are relatively insensitive to the modified nose-gear geometry as long as the tires are allowed to rotate independently.

Corotating twin tires. Tests were also conducted to determine the effect of forcing the twin-tire system to corotate on the magnitude of the cornering forces generated by the tires. The independent twin-tire system was made to corotate by bolting the split rims of each wheel together. The spacing between these wheels was 8 in. from center to center. In figure 14, cornering-force coefficient is plotted as a function of tilt angle, and data for corotating twin tires are compared with data for independently rotating twin tires at both 1.5 and 10 in. of trail. All these data were obtained at a vertical load of 480 lb; hence, each tire for the twin-tire arrangement was operating at 10 percent of its rated load. The data show an increase of up to 500 percent in the sensitivity of the cornering-force coefficient to tilt angle for 1.5 in. of trail when the tires are forced to corotate. For both trail cases, as the tilt angle passed through about 5°, one tire began to leave the ground. This action caused the system to behave more like a single-tire system. At a tilt angle of about 8°, the tire was completely free of the ground, and the twin-tire system acted exactly like the single-tire system. One should note that one of the tires also left the ground during the independent twin-tire tests; however, an inflection point in the curve was not present, since the system was already duplicating single-tire data prior to the tilt angle of 5°.

The increase in sensitivity of the cornering-force coefficient to tilt angle for the corotating twin-tire system is probably influenced by the lateral spacing of the tires. Each tire of the corotating set apparently produces the same moment due to differential slip as its independent

set counterpart. However, there is obviously an additional moment produced as a result of the gross difference in rolling radius between the two tires, and this rolling-radius differential is proportional to the distance between the tire centerlines. Hence, for a given set of corotating twin tires, increasing the separation distance should produce larger cornering-force coefficients for the same tilt angles.

Additional tests were conducted on the corotating twin-tire configuration to evaluate the effect of vertical load on the cornering-force coefficient. The results of these tests are presented in figure 15. Tests were conducted with 1.5 in. of trail at vertical loads of 480, 980, and 1760 lb representing 10, 21, and 37 percent of the rated load on each tire, respectively. The trend of decreasing cornering-force coefficient with increasing vertical load was present as it was with the single-tire configuration. Again, this behavior is similar to that observed in references 4 and 5 for steering forces developed under yawed, rolling conditions.

Concluding Remarks

An experimental investigation was conducted to examine the effects of various parameters on the cornering forces produced by a rolling aircraft tire installed on a tilted, free-swiveling nose gear. A modified airboat equipped with a tricycle landing gear was used as the test vehicle. Parameters studied included tilt angle, trail, tire inflation pressure, rake angle, vertical load, and in the case of a twin-tire configuration, whether or not the tires corotate. These parameters were evaluated by comparing the forces generated by the tire(s) measured perpendicular to the direction of motion as the vehicle was towed in a tilted attitude with the nose gear free to swivel.

The results of this investigation indicate that differential slip across the width of the tire footprint is the mechanism by which cornering forces are generated by a rolling tire installed on a tilted, free-swiveling nose gear.

Generally, cornering-force coefficient increased with increasing tilt angle. Increasing the trail on the nose gear had the effect of nonlinearly decreasing the cornering-force coefficient. It was determined that tire inflation pressure variations had no effect on the cornering-force coefficient as long as the tire was within the design deflection range. Forward rake angle on the nose gear decreased the cornering-force coefficient produced at a given tilt angle. Increasing vertical load decreased the cornering-force coefficient substantially.

A nose gear with independently rotating twin tires will produce cornering-force coefficients comparable to those produced by a single-tire configuration. If the tires are made to corotate, however, the cornering-force coefficients at a given tilt angle can be greatly magnified. The nose-gear configuration most likely to produce the largest cornering forces due to tilt angle would be a corotating twin-tire system with zero trail and rake angle and with the tires widely separated on a free-swiveling system.

NASA Langley Research Center
Hampton, VA 23665
May 14, 1985

Appendix A

Definitions

Tilt angle. Tilt angle on the nose gear is defined as the angle in a vertical plane between the wheel axle and the local surface on which the tire is operating.

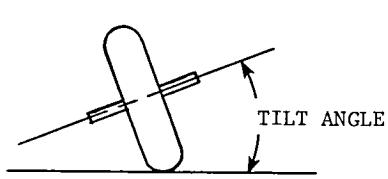

Trail. Trail is defined as the distance between the rotational axis of the strut and the wheel axle at zero yaw angle.

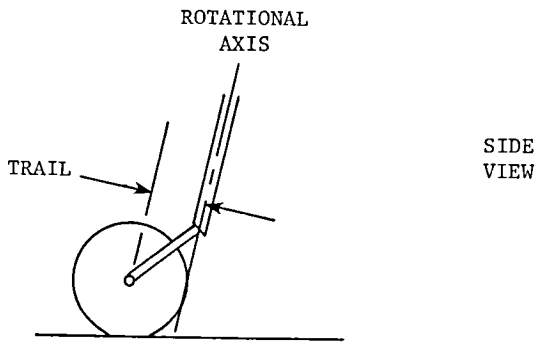

Rake angle. Rake angle is defined as the angle in the vertical plane between the rotational axis of the strut and a line perpendicular to the local surface on which the tire is operating. Note that rake angle can be toward either the rear or the front of the vehicle.

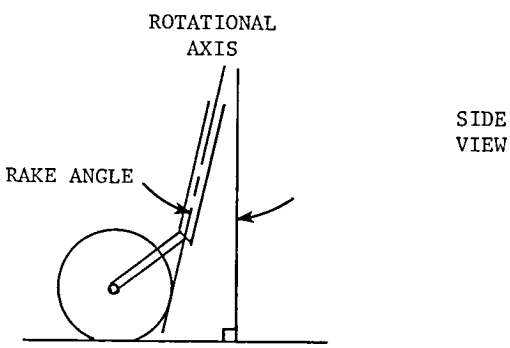

Yaw angle. Yaw angle is defined as the angle in a horizontal plane between the wheel axle and a line perpendicular to the direction of motion of the wheel axle.

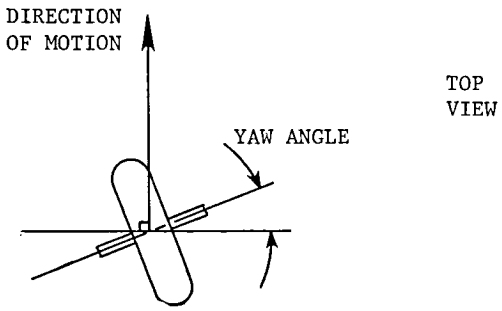

Side force. Side force is defined as a force in the tire footprint parallel to the wheel axle.

Cornering force. Cornering force is defined as the component of the side force that is perpendicular to the direction of motion.

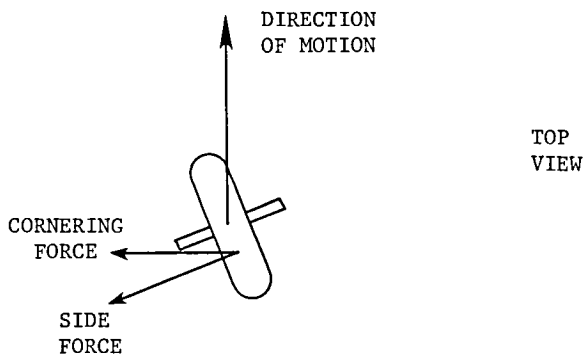

Appendix B

Method of Predicting Torque Due to Differential Slip in the Tire Footprint

The following is a diagram of the footprint of a non-tilted, yawed, rolling tire:

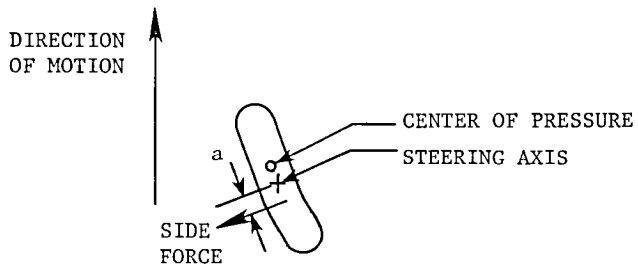

A free-rolling tire has rolling resistance, and the fact that it does not accelerate indicates that the normal force acts forward of the steering axis at the center of pressure. If the tire is tilted, this normal force produces a very small torque, which tends to counteract the torque due to differential slip. This small torque is neglected for the calculations in this paper. Also, the fact that a yawed tire exhibits aligning torque indicates that a side force acts at some distance behind the steering axis; this distance "*a*" is referred to as the side-force moment arm. The torque due to differential slipping, T_{ds}, creates a yaw angle in the tire footprint; consequently, a side force develops that tends to balance this torque produced by the differential slipping.

A method of predicting the torque produced by differential slipping in a single tire has been developed and makes use of the following diagram, which is based on the results of the test shown in figure 7:

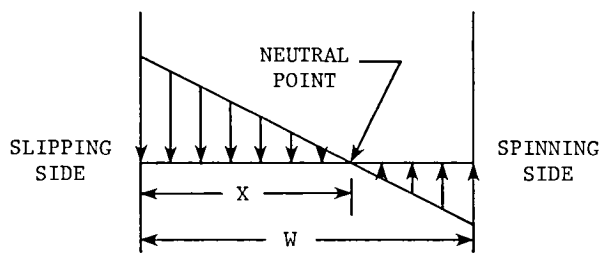

The torque on the tire is the sum of all discrete forces times their distances from the footprint neutral point. Each force is equal to the local normal force, N_{local} (assumed to be constant), times the local friction coefficient, μ_{local}, which is a function of footprint lateral location because of differential slipping. Therefore,

$$T_{ds} = \int_0^{W-X} N_{local}\,\mu_{local}\,dy + \int_0^{X} N_{local}\,\mu_{local}\,dy \tag{B1}$$

where dy is the incremental distance across the tire footprint.

The slip ratio, S, is defined as the difference between ground speed and tire speed divided by the ground speed; hence, a locked, skidding tire would have a slip ratio of 1. Data presented in reference 6 indicate that for slip ratios up to about 0.1, the friction coefficient on a dry surface can be expressed as

$$\mu_{local} = 7.8S \tag{B2}$$

The maximum difference in slip ratio between one edge of the footprint and the other is defined as

$$S_{max} = \frac{W \sin \phi}{R} \tag{B3}$$

where

W	footprint width
ϕ	tilt angle
R	rolling radius of tilted tire

If y is the instantaneous lateral position between the neutral point and the edge of the footprint, then

$$\mu_{local} = \frac{7.8S_{max}y}{W} \tag{B4}$$

Now, substituting the expression for μ_{local} from equation (B4) into equation (B1) gives

$$T_{ds} = \int_0^{W-X} \frac{N_{local}\,7.8S_{max}\,y\,dy}{W}$$

$$+ \int_0^{X} \frac{N_{local}\,7.8S_{max}\,y\,dy}{W} \tag{B5}$$

References

1. Stubbs, Sandy M.: *Landing Characteristics of a Dynamic Model of the HL-10 Manned Lifting Entry Vehicle.* NASA TN D-3570, 1966.
2. Daugherty, Robert H.: *Braking and Cornering Studies on an Air Cushion Landing System.* NASA TP-2196, 1983.
3. Smiley, Robert F.; and Horne, Walter B.: *Mechanical Properties of Pneumatic Tires With Special Reference to Modern Aircraft Tires.* NASA TR R-64, 1960. (Supersedes NACA TN 4110.)
4. Vogler, William A.; and Tanner, John A.: *Cornering Characteristics of the Nose-Gear Tire of the Space Shuttle Orbiter.* NASA TP-1917, 1981.
5. Tanner, John A.; Stubbs, Sandy M.; and McCarty, John L.: *Static and Yawed-Rolling Mechanical Properties of Two Type VII Aircraft Tires.* NASA TP-1863, 1981.
6. Tanner, John A.; Stubbs, Sandy M.; Dreher, Robert C.; and Smith, Eunice G.: *Dynamics of Aircraft Antiskid Braking Systems.* NASA TP-1959, 1982.

TABLE I. SUMMARY OF TEST CONDITIONS AND RESULTS

Run no.	Tilt angle, deg	Trail, in.	Inflation pressure, psi	Rake angle, deg	Vertical load, lb	Percent of rated load	Independent twin tires	Corotating twin tires	Measured cornering force, lb	Corrected cornering force, lb	Cornering-force coefficient
1	0	0	24	0	480	20			0	0	0
2	1	0	24	0	480	20			57	55	0.11
3	2	0	24	0	480	20			75	71	0.15
4	3	0	24	0	480	20			110	103	0.21
5	4	0	24	0	480	20			132	122	0.25
6	5	0	24	0	480	20			182	170	0.35
7	6	0	24	0	480	20			148	133	0.28
8	7	0	24	0	480	20			238	221	0.46
9	8	0	24	0	480	20			288	268	0.56
10	9	0	24	0	480	20			272	250	0.52
11	10	0	24	0	480	20			272	247	0.51
12	2	0	24	0	480	20			3	*3	0.01
13	6	0	24	0	480	20			8	*8	0.02
14	8	0	24	0	480	20			25	*25	0.05
15	10	0	24	0	480	20			30	*30	0.06
16	3	0	24	0	480	20			88	*88	0.18
17	6	0	24	0	480	20			178	*178	0.37
18	8	0	24	0	480	20			228	*228	0.48
19	9	0	24	0	480	20			260	*260	0.54
20	10	0	24	0	480	20			314	*314	0.65
21	2	1.5	24	0	480	20			51	46	0.10
22	4	1.5	24	0	480	20			95	85	0.18
23	6	1.5	24	0	480	20			133	118	0.25
24	8	1.5	24	0	480	20			170	150	0.31
25	10	1.5	24	0	480	20			212	187	0.39
26	2	10	24	0	480	20			38	33	0.07
27	4	10	24	0	480	20			75	65	0.14
28	6	10	24	0	480	20			91	76	0.16

*Dolly tests. Therefore, measured and corrected values are the same.

TABLE I. Continued

Run no.	Tilt angle, deg	Trail, in.	Inflation pressure, psi	Rake angle, deg	Vertical load, lb	Percent of rated load	Independent twin tires	Corotating twin tires	Measured cornering force, lb	Corrected cornering force, lb	Cornering-force coefficient
29	8	10	24	0	480	20			123	103	0.21
30	10	10	24	0	480	20			165	140	0.29
31	10	10	24	0	480	20			142	117	0.24
32	3	0	60	0	480	20			101	93	0.19
33	6	0	60	0	480	20			173	158	0.33
34	10	0	60	0	480	20			315	290	0.60
35	5	1.5	12	0	480	20			89	76	0.16
36	10	1.5	12	0	480	20			170	145	0.30
37	2	1.5	24	10	480	20			43	38	0.08
38	4	1.5	24	10	480	20			75	65	0.14
39	5	1.5	24	10	480	20			92	80	0.17
40	6	1.5	24	10	480	20			115	100	0.21
41	5	1.5	45	0	980	42			159	147	0.15
42	10	1.5	45	0	980	42			305	280	0.29
43	2	1.5	45	0	1760	75			88	83	0.05
44	5	1.5	45	0	1760	75			208	196	0.11
45	6	1.5	45	0	1760	75			255	240	0.14
46	8	1.5	45	0	1760	75			322	302	0.17
47	10	1.5	45	0	1760	75			412	387	0.22
48	2	1.5	24	0	480	10	X		48	43	0.09
49	4	1.5	24	0	480	10	X		87	77	0.16
50	6	1.5	24	0	480	10	X		115	100	0.21
51	8	1.5	24	0	480	10	X		154	134	0.28

TABLE I. Concluded

Run no.	Tilt angle, deg	Trail, in.	Inflation pressure, psi	Rake angle, deg	Vertical load, lb	Percent of rated load	Independent twin tires	Corotating twin tires	Measured cornering force, lb	Corrected cornering force, lb	Cornering-force coefficient
52	10	1.5	24	0	480	10	X		200	175	0.36
53	2	10	24	0	480	10	X		34	29	0.06
54	4	10	24	0	480	10	X		85	75	0.16
55	6	10	24	0	480	10	X		96	81	0.17
56	8	10	24	0	480	10	X		122	102	0.21
57	10	10	24	0	480	10	X		159	134	0.28
58	1	1.5	24	0	480	10		X	132	130	0.27
59	2	1.5	24	0	480	10		X	188	183	0.38
60	3	1.5	24	0	480	10		X	287	280	0.58
61	4	1.5	24	0	480	10		X	352	342	0.71
62	5	1.5	24	0	480	10		X	351	339	0.71
63	6	1.5	24	0	480	10		X	277	262	0.55
64	8	1.5	24	0	480	10		X	177	157	0.33
65	10	1.5	24	0	480	10		X	189	164	0.34
66	2	10	24	0	480	10		X	78	73	0.15
67	4	10	24	0	480	10		X	114	104	0.22
68	5	10	24	0	480	10		X	115	103	0.21
69	6	10	24	0	480	10		X	120	105	0.22
70	7	10	24	0	480	10		X	115	98	0.20
71	8	10	24	0	480	10		X	127	107	0.22
72	10	10	24	0	480	10		X	154	129	0.27
73	2	1.5	45	0	980	21		X	122	117	0.12
74	4	1.5	45	0	980	21		X	286	276	0.28
75	6	1.5	45	0	980	21		X	406	391	0.40
76	2	1.5	45	0	1760	37		X	190	185	0.11
77	4	1.5	45	0	1760	37		X	348	338	0.19
78	6	1.5	45	0	1760	37		X	500	485	0.28

L-84-3913

Figure 1. Test vehicle in tilted attitude of 10°.

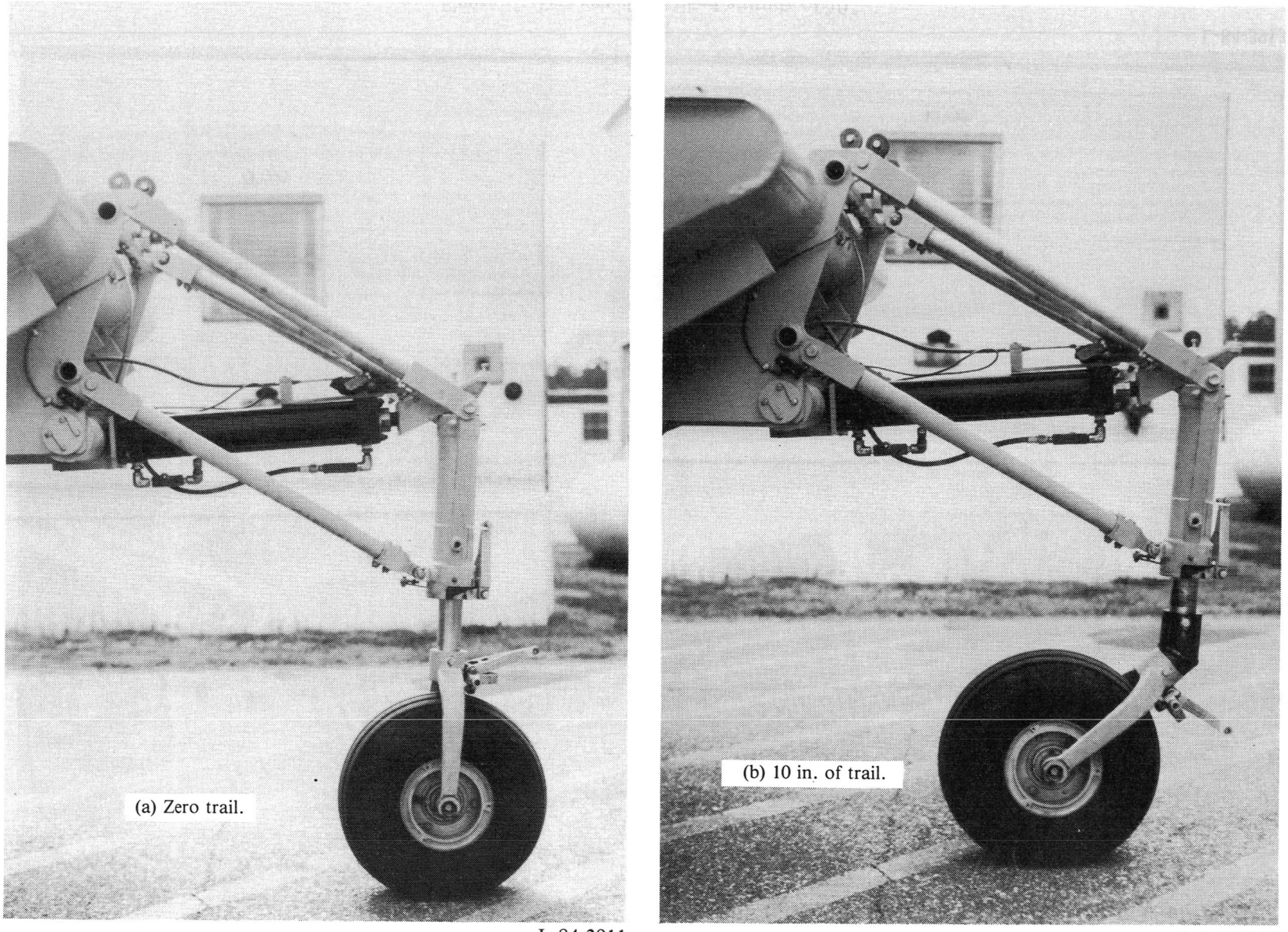

L-84-3911

L-84-39116

Figure 2. Nose-gear trail assemblies.

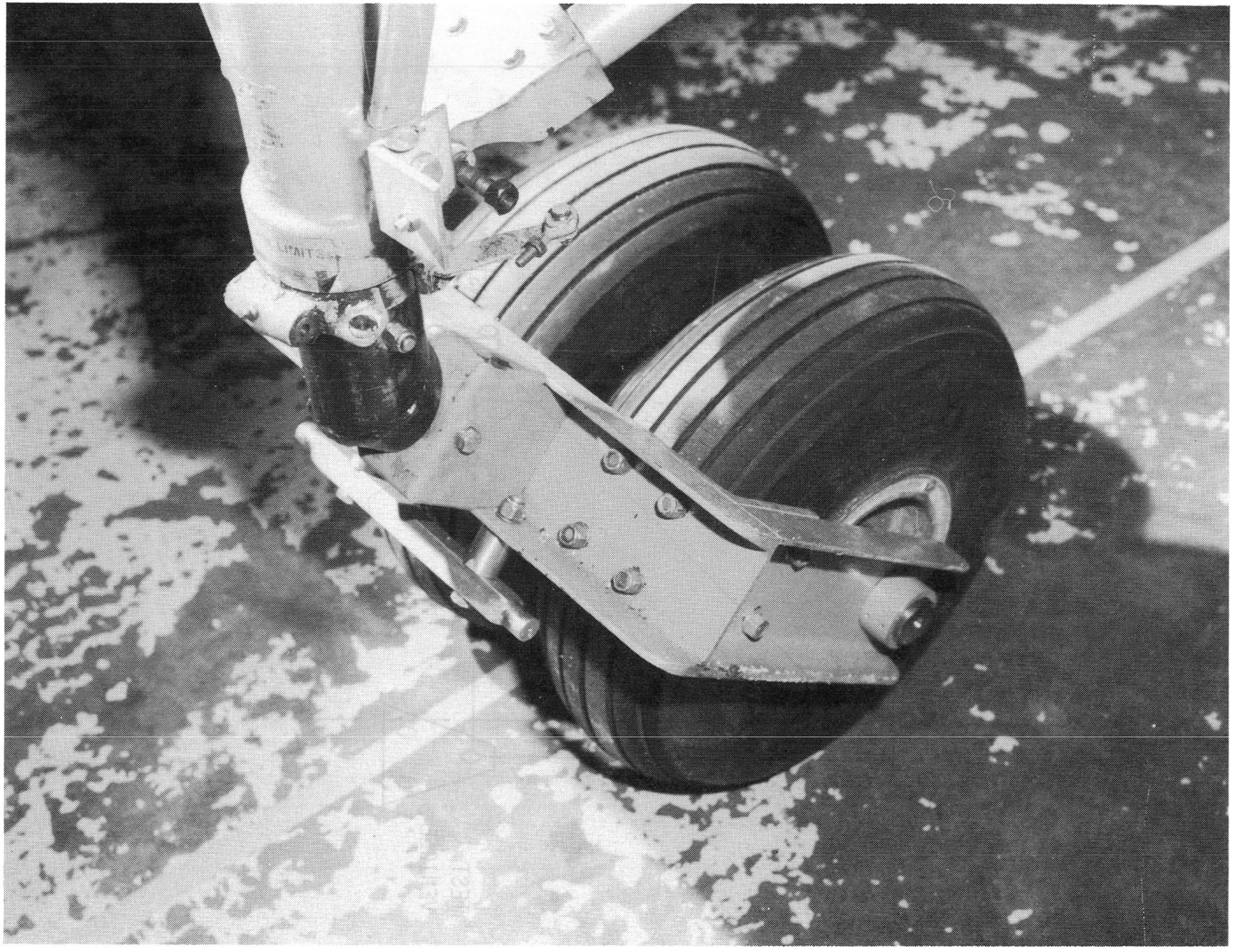

L-84-6788

Figure 3. Twin-tire test assembly with 10 in. of trail.

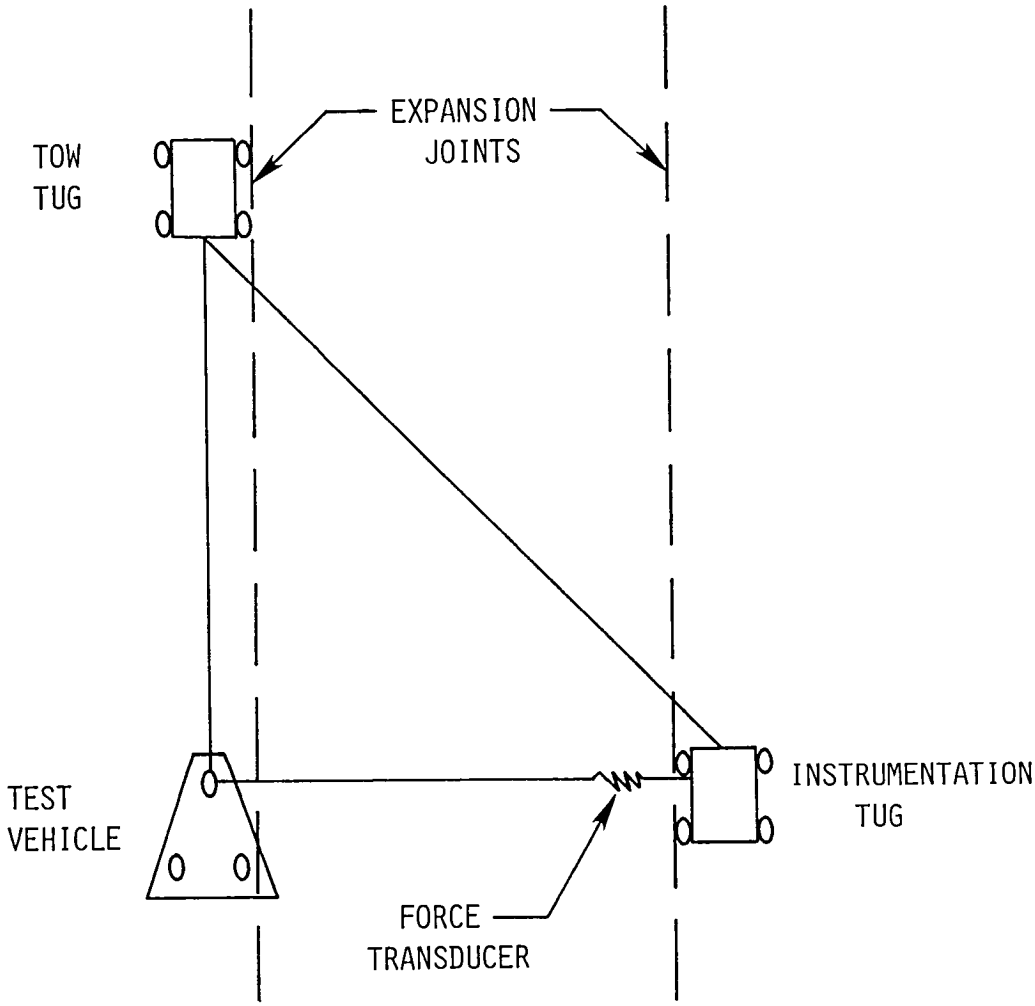

Figure 4. Schematic of tow test setup.

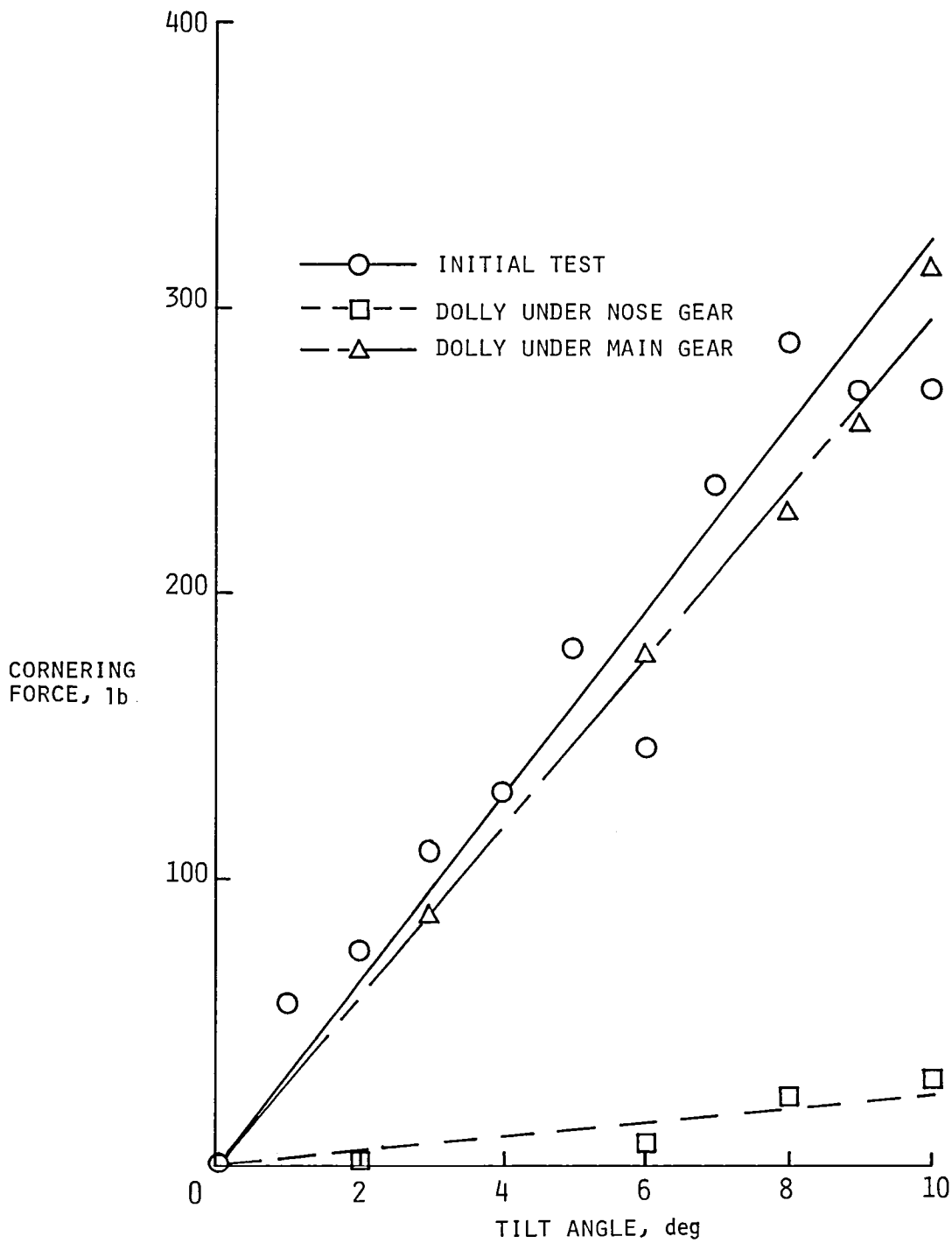

Figure 5. Variation of cornering force as a function of tilt angle for various test configurations.

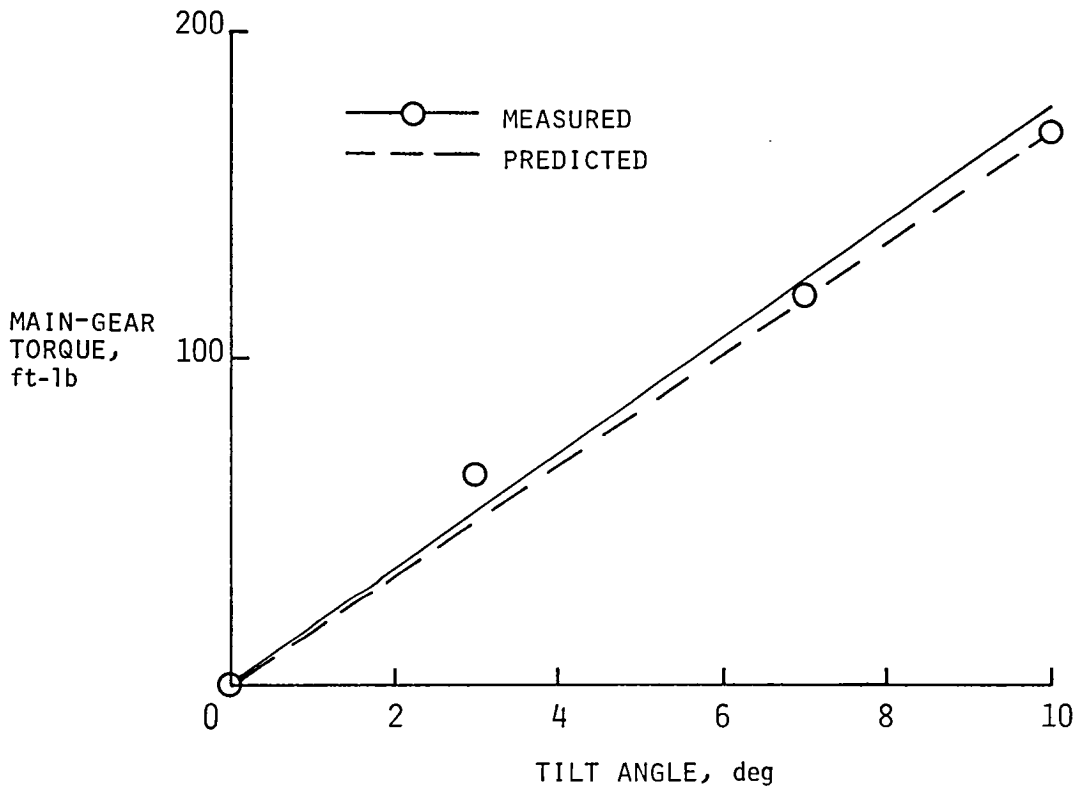

Figure 6. Variation of torque generated by main-gear tire as a function of tilt angle.

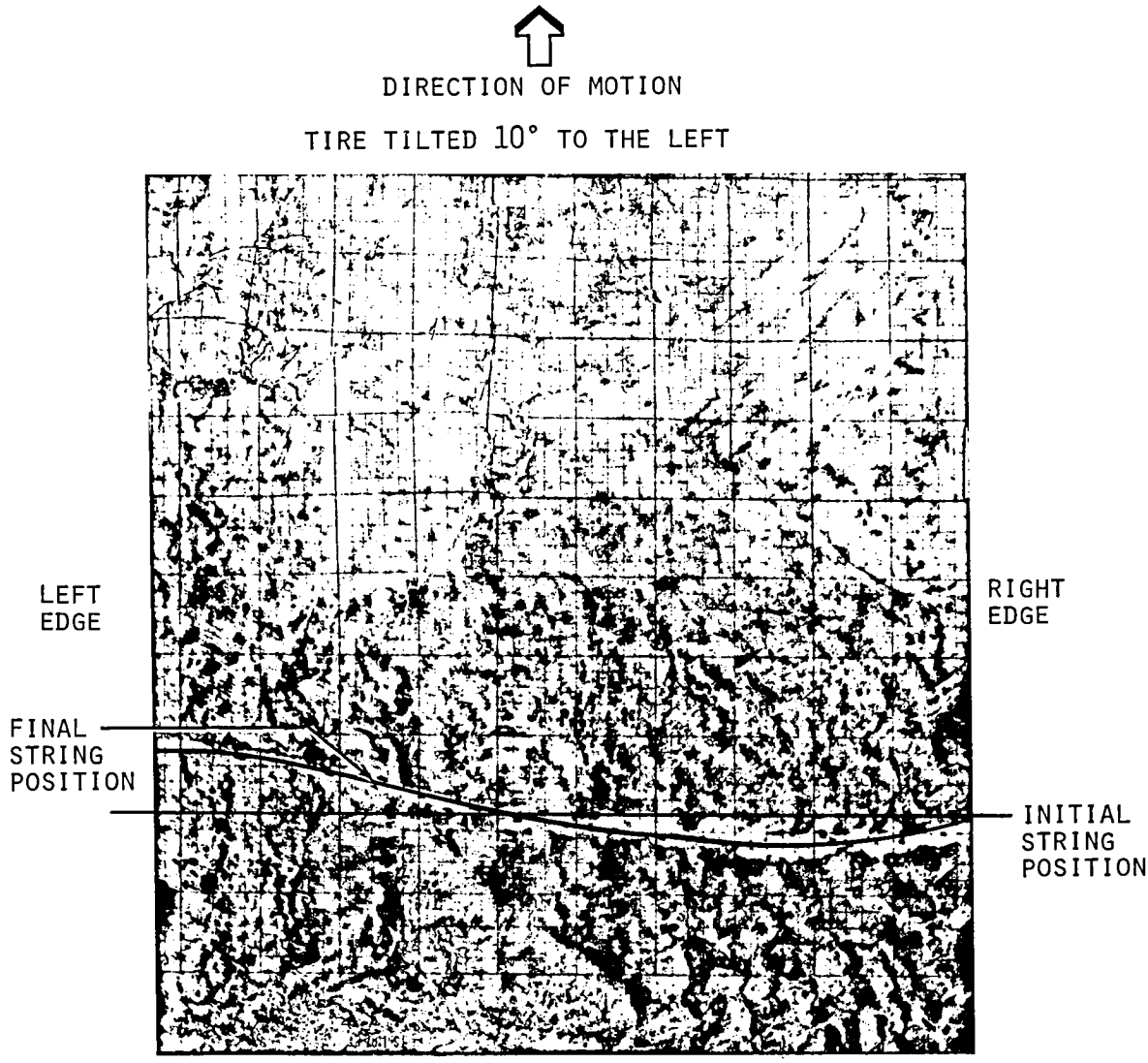

Figure 7. Illustration of differential slip in footprint of tilted, rolling tire.

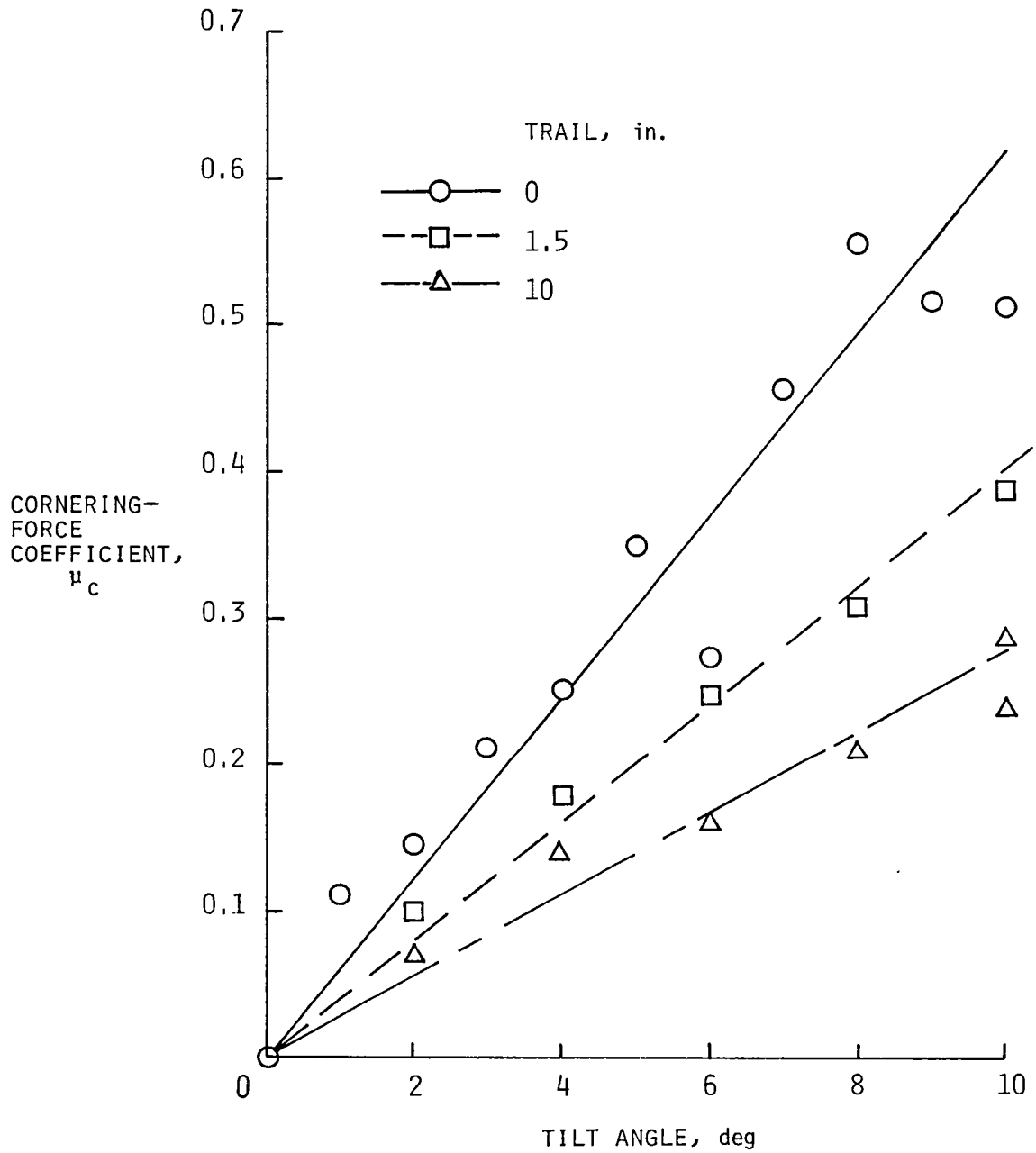

Figure 8. Variation of cornering-force coefficient as a function of tilt angle for various nose-gear trails.

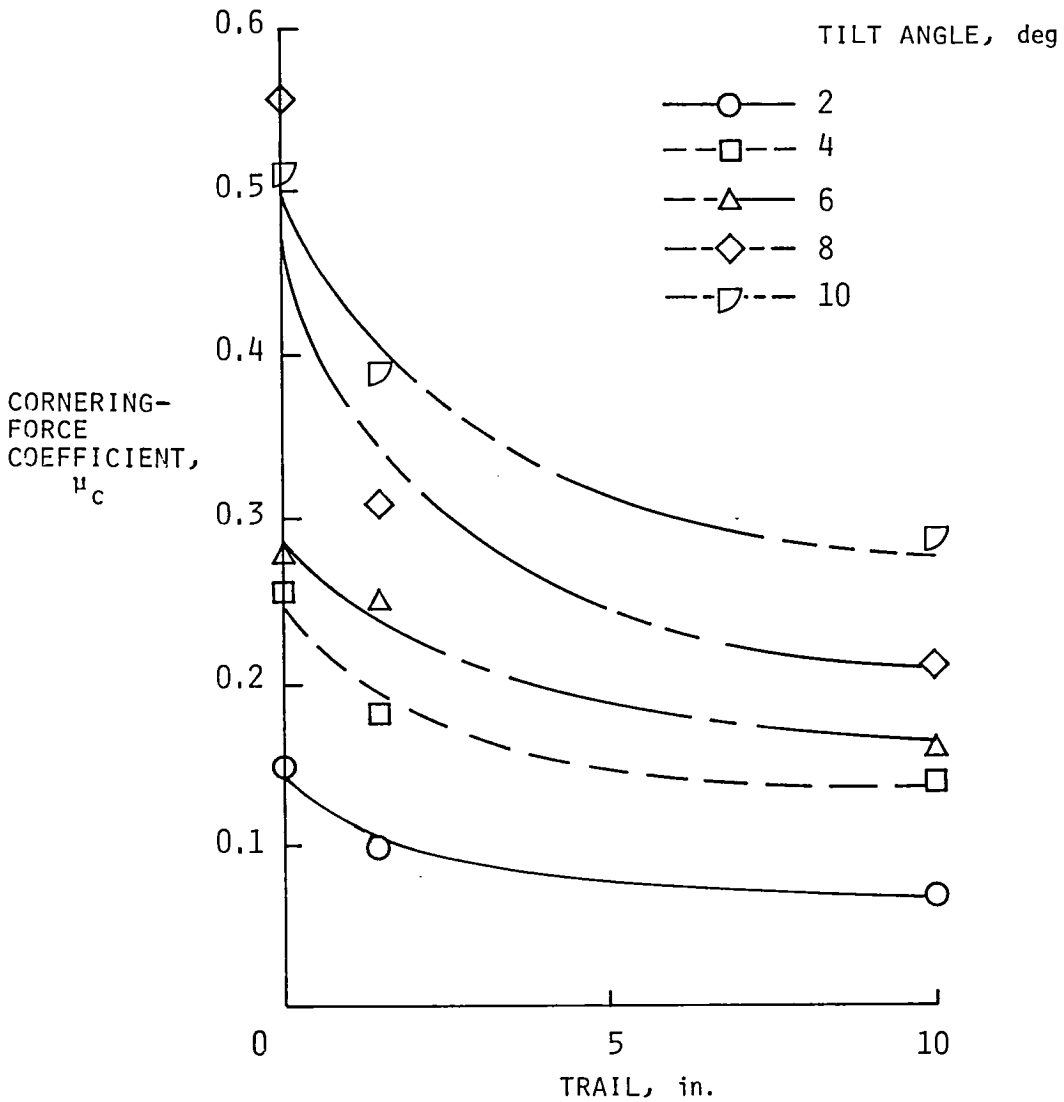

Figure 9. Variation of cornering-force coefficient as a function of trail for various tilt angles.

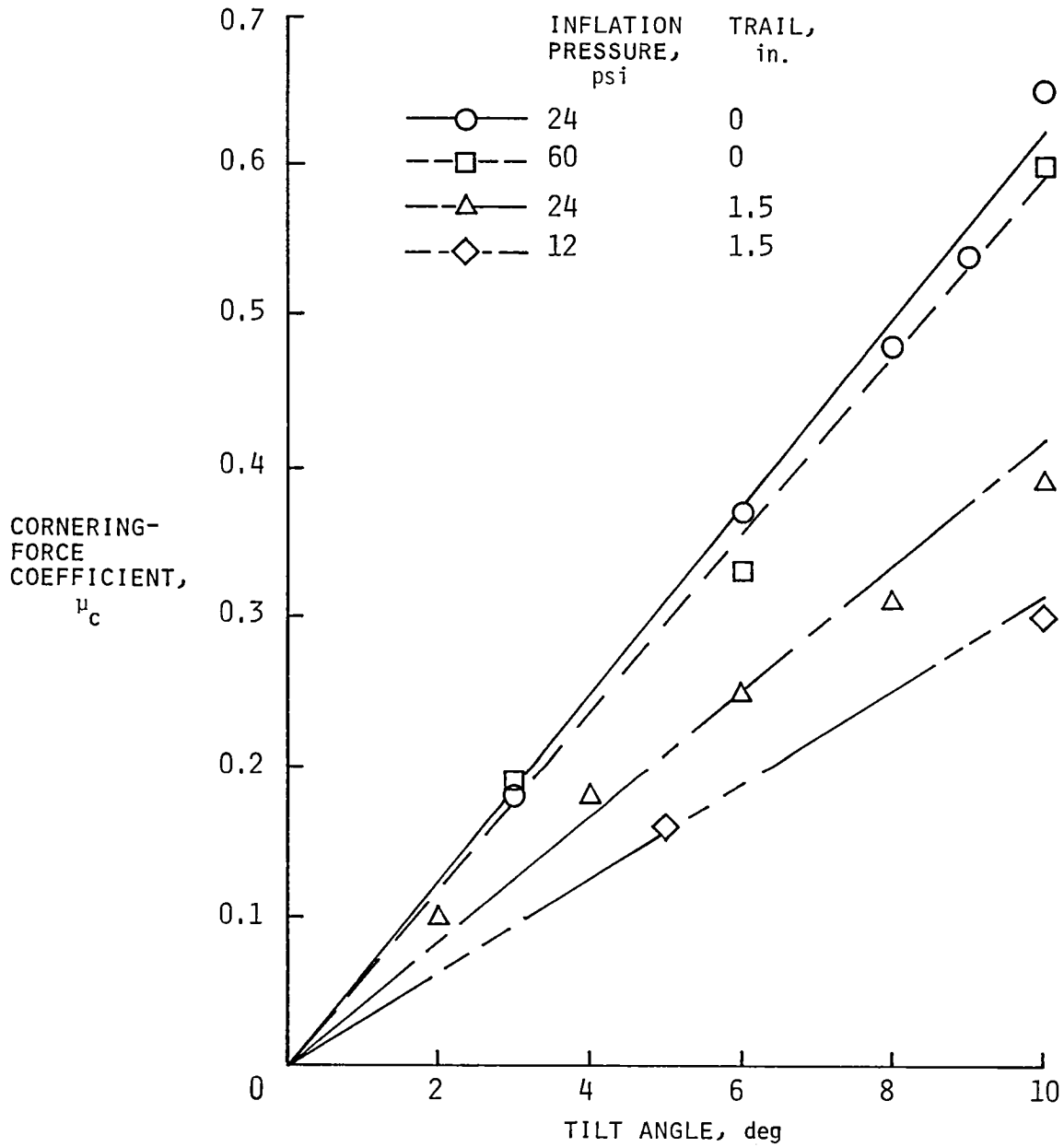

Figure 10. Variation of cornering-force coefficient as a function of tilt angle for various inflation pressures and trails.

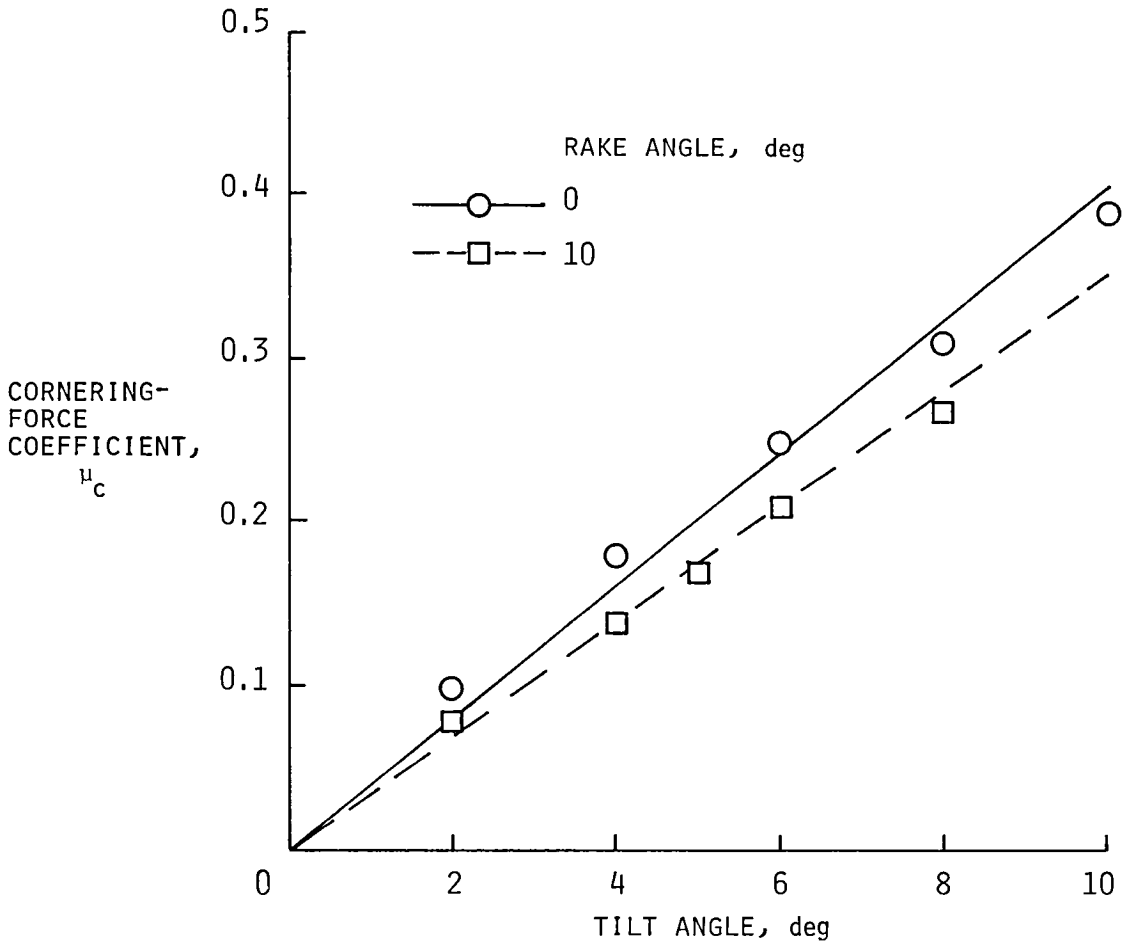

Figure 11. Variation of cornering-force coefficient as a function of tilt angle for various rake angles. Trail = 1.5 in.

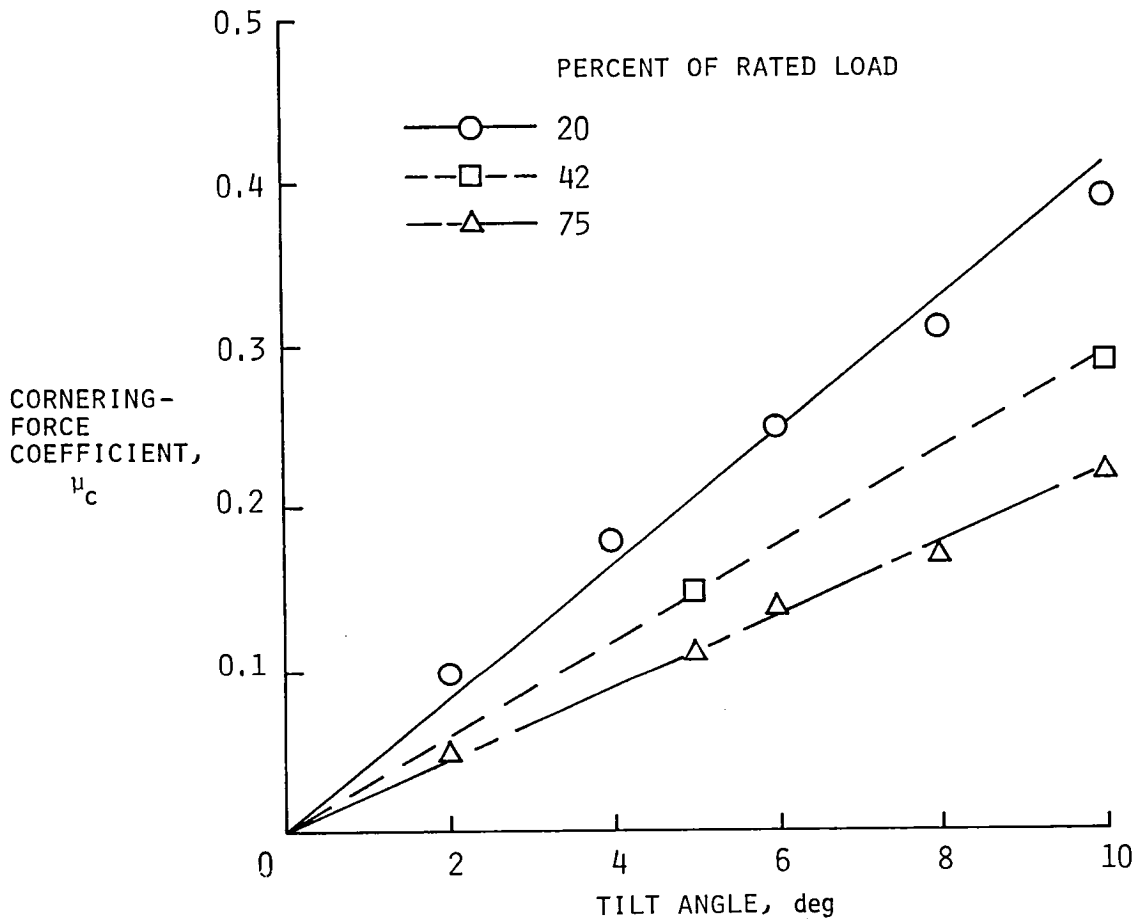

Figure 12. Variation of cornering-force coefficient as a function of tilt angle for different vertical loads. Trail = 1.5 in.

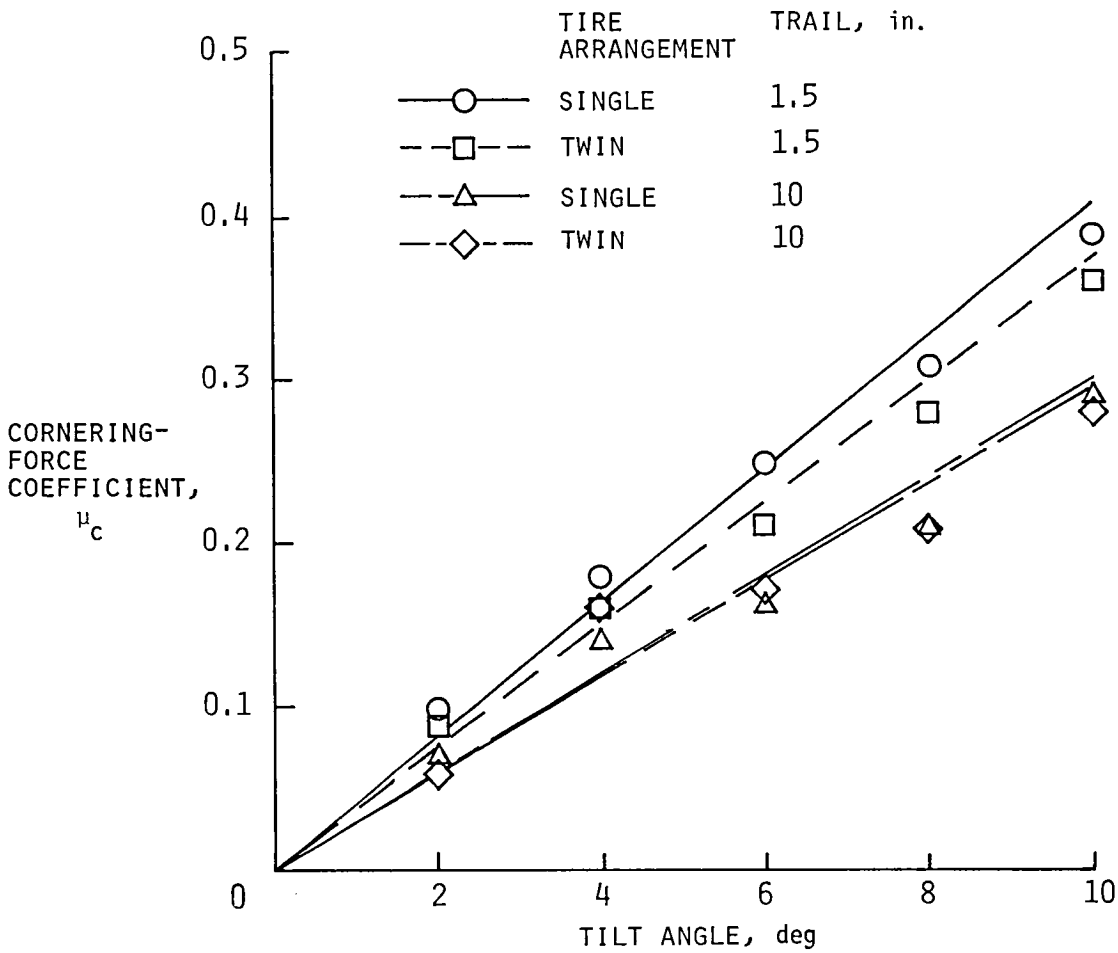

Figure 13. Variation of cornering-force coefficient as a function of tilt angle for various tire arrangements and trails.

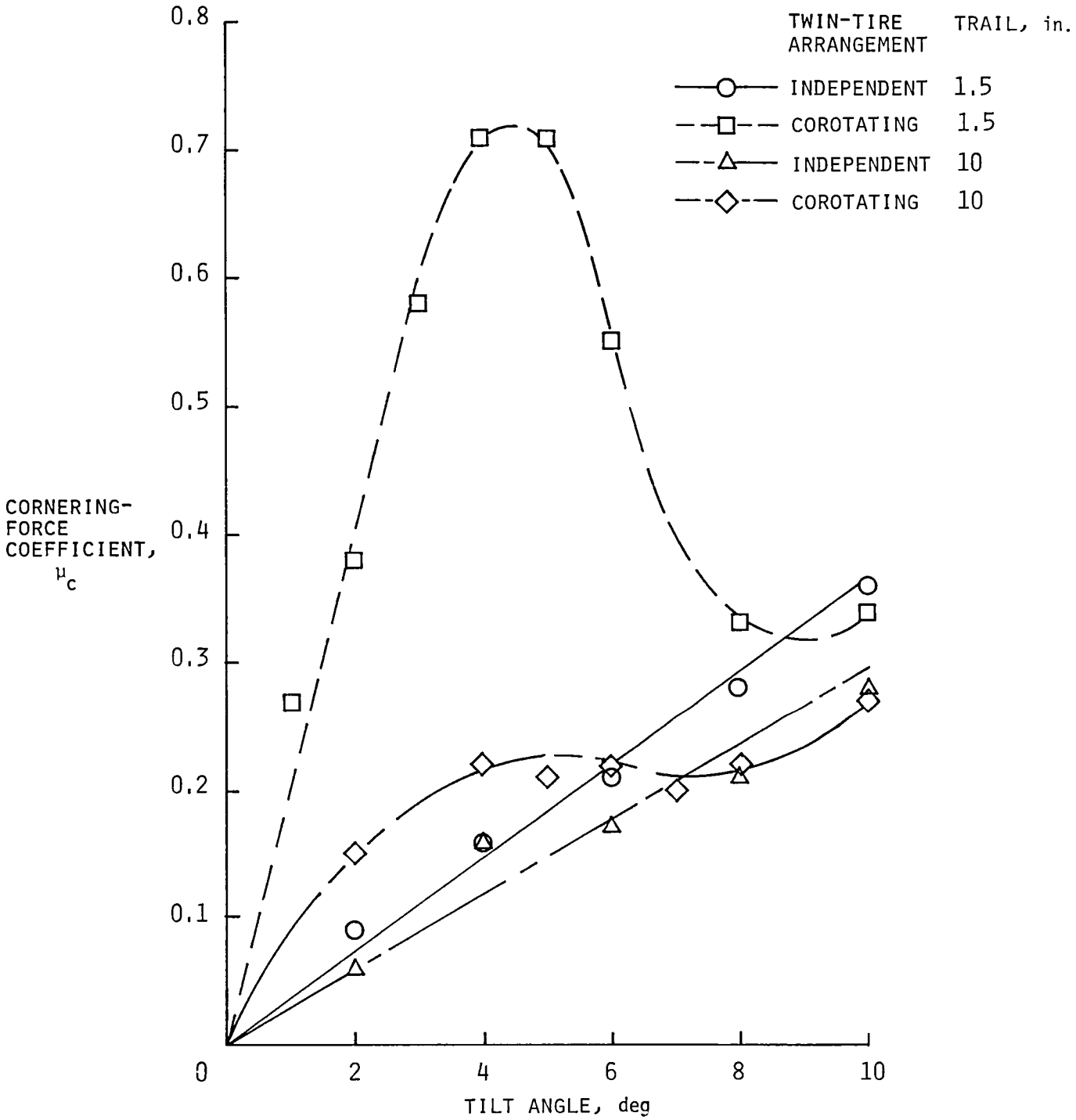

Figure 14. Variation of cornering-force coefficient as a function of tilt angle for various twin-tire arrangements and trails.

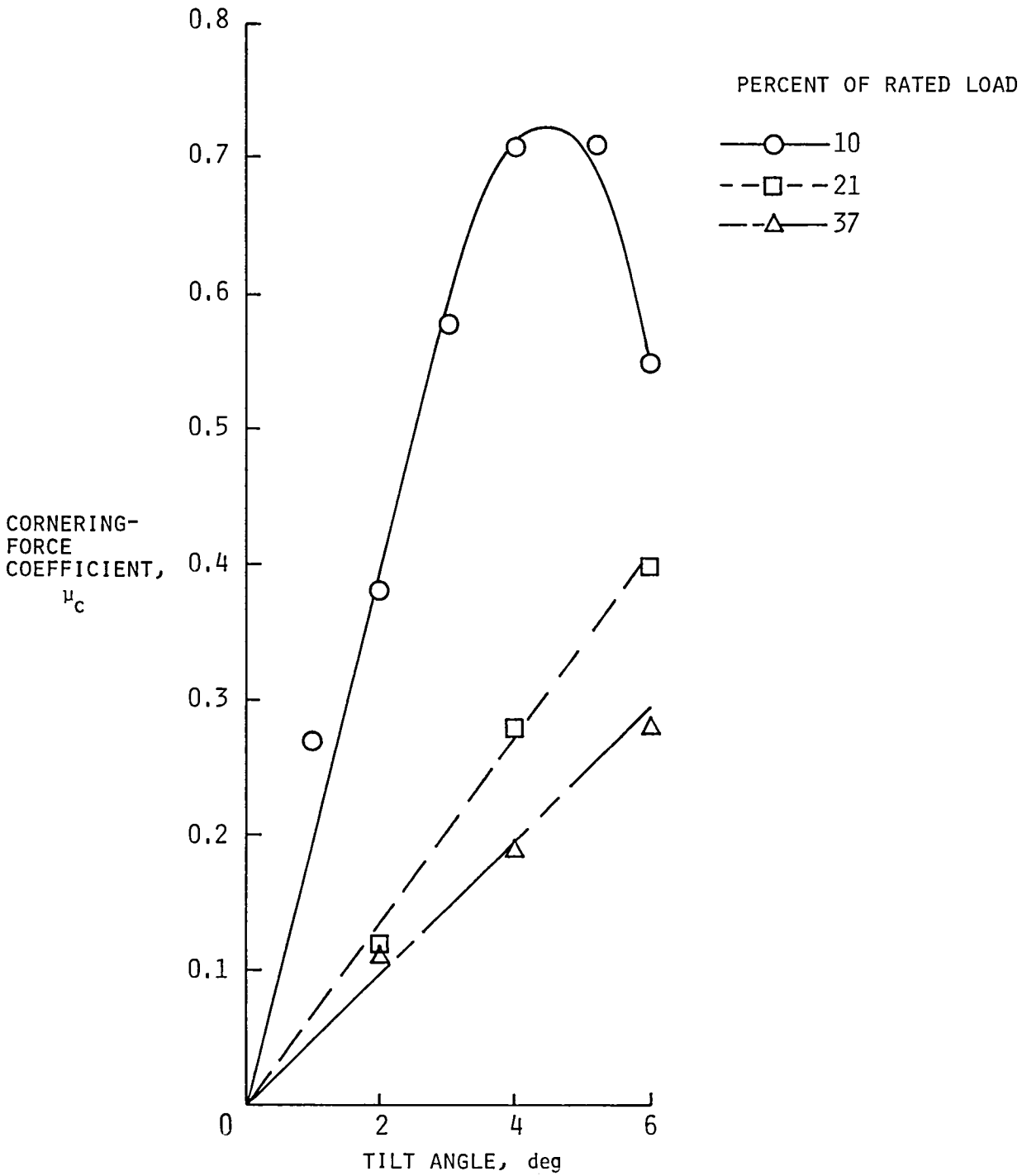

Figure 15. Variation of cornering-force coefficient as a function of tilt angle for a corotating twin-tire arrangement at different vertical loads.

1. Report No.	2. Government Accession No.	3. Recipient's Catalog No.
NASA TP-2481		

4. Title and Subtitle	5. Report Date
A Study of the Cornering Forces Generated by Aircraft Tires on a Tilted, Free-Swiveling Nose Gear	October 1985
	6. Performing Organization Code 505-45-14-01
7. Author(s) Robert H. Daugherty and Sandy M. Stubbs	8. Performing Organization Report No. L-15954
	10. Work Unit No.
9. Performing Organization Name and Address NASA Langley Research Center Hampton, VA 23665	11. Contract or Grant No.
	13. Type of Report and Period Covered Technical Paper
12. Sponsoring Agency Name and Address National Aeronautics and Space Administration Washington, DC 20546	14. Sponsoring Agency Code

15. Supplementary Notes

16. Abstract

An experimental investigation was conducted at the NASA Langley Research Center to study the effect of various parameters on the cornering forces produced by a rolling aircraft tire installed on a tilted, free-swiveling nose gear. The parameters studied included tilt angle, trail, tire inflation pressure, rake angle, vertical load, and whether or not a twin-tire configuration corotates. These parameters were evaluated by measuring the cornering force produced by an aircraft tire installed on the nose gear of a modified vehicle as it was towed slowly. Cornering-force coefficient increased with increasing tilt angle. Increasing trail or rake angle decreased the magnitude of the cornering-force coefficient. Tire inflation pressure had no effect on the cornering-force coefficient. Increasing vertical load decreased the cornering-force coefficient. When the tires of a twin-tire system rotated independently, the cornering-force coefficients were the same as those for the single-tire configuration. When the twin-tire system was made to corotate, however, the cornering-force coefficients increased significantly.

17. Key Words (Suggested by Author(s))	18. Distribution Statement
Aircraft tire Cornering force Tilt angle Corotation	Unclassified—Unlimited Subject Category 39

19. Security Classif. (of this report)	20. Security Classif. (of this page)	21. No. of Pages	22. Price
Unclassified	Unclassified	28	A03

N-305

For sale by the National Technical Information Service, Springfield, Virginia 22161

NASA-Langley, 1985

National Aeronautics and
Space Administration
Code NIT-3

Washington, D.C.
20546-0001

Official Business
Penalty for Private Use, $300

BULK RATE
POSTAGE & FEES PAID
NASA Washington, DC
Permit No. G-27

NASA

POSTMASTER: **If Undeliverable (Section 158 Postal Manual) Do Not Return**